ISSN 0915-633X

NATIONAL INSTITUTE FOR FUSION SCIENCE

The Origin of Collisionless Dissipation in Magnetic Reconnection

M. Tanaka

(Received – Sep. 6, 1993)

NIFS-245

Sep. 1993

RESEARCH REPORT
NIFS Series

NAGOYA, JAPAN

The Origin of Collisionless Dissipation in Magnetic Reconnection

Motohiko Tanaka

National Institute for Fusion Science
Nagoya 464-01, Japan

Abstract

The mechanism of collisionless reconnection in magnetized plasmas is studied in terms of coalescence of two flux tubes using implicit particle simulation. The motional electric field resulting from magnetic attraction generates the non-MHD (magneto-hydrodynamic), scalar electrical potential of a quadrupole configuration across the x-point. This electric field transports the plasma and magnetic flux into and out of the diffusion layer, and also accelerates the finite mass electrons to produce the current $J_{\|}$ along the helical magnetic field. These processes provide equivalent dissipation which makes magnetic reconnection possible in collisionless magnetized plasmas.

Keywords: magnetic reconnection, collisionless dissipation, magnetized plasma, implicit particle simulation

The magnetic reconnection is believed to play an important role in changing topology of magnetic field and converting its energy to plasma directed and thermal energies in fusion and astrophysical plasmas. A global study of the magnetic reconnection is usually done using magnetohydrodynamic (MHD) equations combined with dissipation of plasma current. But, the origin of "collisionless" dissipation which needs to be much larger than that of the classical Coulomb collision has remained a mystery of plasma physics for many years.

Previous theoretical studies of magnetic reconnection in semi-collisional regime started from a reduced set of equations where a generalized Ohm's law with electron inertia effect[1,2] or hyper-resistivity[3] was assumed. To study nonlinear kinetic stages of magnetic reconnection, electromagnetic particle simulations[4,5] and an implicit particle simulation[6] were carried out for unmagnetized or weakly magnetized plasmas. For the purpose of elucidating the mechanism of collisionless reconnection in "magnetized" plasmas, we show in this paper simulation results of coalescence of two flux tubes by means of 2-D electromagnetic, implicit particle simulation code (HIDENEK) which includes electron inertia effects[7].

A special feature here is the presence of the toroidal magnetic field as is the case with high-temperature, non-resistive plasmas found in magnetic fusion devices[8,9] and the solar corona[10]. We use the electron inertia length c/ω_{pe} as the unit of length, which is expected to be the characteristic length of collisionless reconnection[1,2]. For the TFTR parameters[8], i.e., $n = 5\times10^{13}/\mathrm{cm}^3$, $B = 4\mathrm{T}$ and $T_i = 7\mathrm{keV}$, we have $c/\omega_{pe} \sim 7.5\times10^{-2}\mathrm{cm}$ and the ion gyroradius $\rho_i \sim 0.31\mathrm{cm}$, hence, $\rho_i/(c/\omega_{pe}) \sim 4$. The simulation is done in this parameter regime. Also, under the present geometry, the current-carrying flux tubes attract each other which naturally leads to reconnection without a driving electric field. Moreover, the reconnection electric field is orthogonal to the convection electric field which facilitates identification of the reconnection mechanism.

A numerical advantage of the implicit particle simulation[7,11] is realization of large time-and-space scales, $L \geq c/\omega_{pe}$ and $\omega_{pe}\tau \gg 1$. Full particle dynamics is kept for ions, whereas the guiding-center drift formula is adopted to the perpendicular motion

of electrons. Along the magnetic field, by contrast, the electrons are treated as particles with finite mass. A detailed description of the algorithm and mathematical-numerical proofs of the implicit particle code HIDENEK are documented in Ref.7. In order to have a better spatial resolution of the "diffusion layer" that is formed at the center of the system, $x \cong \frac{1}{2}L_x$, spatially-fixed uneven meshes are adopted in the x-direction. Furthermore, to keep the particle fluctuations in a low level, one giant particle is split into three small particles with the $(q/m)_j$ ratio fixed when the giant particle has entered the fine-mesh region. On the other hand, to avoid physics ambiguity, the particles once split are not coalesced to one giant particle even when they leave the fine-mesh region.

To make a simulation, a charge-neutral plasma is initially set up in a doubly-periodic Cartesian box of two dimensions. The system size is $L_x = 400c/\omega_{pe}$, $L_z = 300c/\omega_{pe}$ with 160×72 cells. The grid interval is $\Delta x \cong 1.1c/\omega_{pe}$ for the central part (53 cells) and $\Delta x \cong 3.2c/\omega_{pe}$ for the rest. The mesh size in the z-direction is equal, $\Delta z \cong 4.1c/\omega_{pe}$. The same number of ions and electrons (64 ions/cell) are loaded homogeneously, and their velocities are generated according to the Boltzman distribution functions. An initial drift in the positive y-direction is given to the ions that reside in two square areas to produce a pair of flux tubes. The electrons are drifting slowly at an equal velocity to shield the magnetic field of the flux tubes from their images in the periodic system. Physical parameters chosen are the mass ratio $m_i/m_e = 100$, the strength of the toroidal (y-direction) magnetic field $\omega_{ce}^{(0)}/\omega_{pe} = 1$, electron beta value $\beta_e = 8\pi n T_e/B^2 = 0.04$, and the temperature ratio $T_i/T_e = 1$. The ion gyroradius becomes $\rho_i \cong 2c/\omega_{pe}$, and the time step is chosen to be $\omega_{pe}\Delta t = 50$.

Figure 1 shows the poloidal magnetic flux function Ψ calculated by $\mathbf{B}_p = \nabla \times (\Psi \hat{y})$ and the y-component of the ion current J_{iy} at the times $t/\tau_A = 0$, 1.6 and 3.1, where $\tau_A = \frac{1}{2}d/v_{Ap} \sim 3200\omega_{pe}^{-1}$ with $d = 160c/\omega_{pe}$ the initial distance of two flux tubes and $v_{Ap} = B^{(0)}/(4\pi m_i n)^{1/2} \sim 0.025c$. The isolated two flux tubes attract each other with magnetic tension produced by their positive current J_{iy}, and are squeezed at their contact surface until magnetic reconnection sets in at $t/\tau_A \cong 1.5$. The magnetic reconnection is detected by measuring the amount of isolated poloidal magnetic flux

which is contained in the flux tube. The initial number of isolated contours of the magnetic flux function, five, decreases to two at $t/\tau_A = 3.1$, as shown in the figure. In the late stage, flux merging slows down and it becomes hard to find a well-defined x-point at $t/\tau_A \sim 5$; one flux tube has been absorbed by the other. The total poloidal magnetic flux is nearly a conserved quantity, as is conserved within three percent during the present simulation run.

The ion current shown in Fig.1 gradually pinches and its contours become rather round-shaped because the initially given pressure profile is homogeneous. As the two flux tubes collide, a negative current that divides the positive currents of the flux tubes rapidly develops in the gap between them. The total amount of the negative current reaches its maximum around $t/\tau_A \cong 1.5$ and is dominated by the electron current J_{ey}, i.e., $J_{ey}/J_{iy} \sim 10$. At this time, the negative current occupies the whole separatrix region around the x-point. But, the area of the negative current shrinks drastically for $t/\tau_A \geq 2.2$, and covers only a narrow region including the x-point. The negative gap between the flux tubes is almost filled by $t/\tau_A \cong 3$.

The time history of isolated magnetic flux is shown in Fig.2. The amount of the isolated poloidal magnetic flux is measured by the difference of the peak value of the flux function in the flux tubes (averaged) and that on the separatrix. For the early phase, the amount of the isolated magnetic flux stays almost the same. Around $t/\tau_A \cong 1.5$, merging of the magnetic fluxes starts suddenly. This corresponds to the time when two groups of the electrons that initially reside with the current-carrying ions first collide at the x-point, trailing those ions behind. Also the width of the "diffusion layer" has become comparable to the electron inertia length as shown in Fig.3. During the reconnection, the amount of the isolated fluxes decreases linearly in time. This is apparently the Sweet-Parker type reconnection[12,13] $\Psi \propto t$ (though the electric field plays a role here). The magnetic reconnection continues until most of the flux contained in the two flux tubes has merged owing to the presence of the toroidal magnetic field.

It is important to point out that the non-MHD electric field with divergence ($\nabla \cdot \mathbf{E} = \rho \neq 0$) plays a major role in the collisionless magnetic reconnection. The electric field,

the scalar potential and the ion current in the poloidal plane are displayed in Fig.3 for $t/\tau_A \cong 1.6$. A strong electric field, E_z, has been generated laterally across the flux tubes in association with convective motion of the flux tube plasmas toward the x-point. The electric field becomes divergent because the area of the convective motion is spatially limited to within the flux tubes. This is better understood in the electrical potential φ of Fig.3(b) calculated by $\mathbf{E}_p = -\nabla\varphi$. Obviously, the charge redistribution has occurred in a quadrupole configuration in the regions apart from the x-point; the positive charge accumulates in the second and fourth quadrants with the origin at the x-point, while the electrons in the first and third quadrants. The x-point becomes a saddle point of the potential; the poloidal electric field vanishes there.

As a consequence of the charge redistribution, an even stronger electric field, E_x, appears automatically in the gap between the two flux tubes, pointing to the downward x-direction for $z < \frac{1}{2}L_z$ and to the upward direction for $z > \frac{1}{2}L_z$. It is noted that the width of the "diffusion layer" l_x is much smaller than its length l_z, i.e., $l_x \ll l_z$, hence, $E_x \gg E_z$. The ion current in the poloidal plane is shown in Fig.3(c). The ions flowing vertically toward the x-point from top and bottom are diverted to the lateral direction. The ion and electron currents nearly cancel each other in the poloidal plane. The outward velocity observed for Fig.3 is $V_z/c = 0.022c$ ($\sim v_{Ap}$), which coincides with $V_{E\times B} \sim 0.023c$ calculated by the measured electric field. Thus, the E_x electric field is strong enough to accelerate the incoming plasmas above the (poloidal) Alfven speed and to remove them from the vicinity of the x-point.

Another important observation about the electric field is the "reconnection" electric field E_y (out of the plane component) that is induced in the "diffusion layer" by Faraday's law. At the onset of the reconnection, the width of the diffusion layer has become narrow compared with the MHD scales, $l_x \leq 5c/\omega_{pe}$, as shown in the magnified plots of Fig.3(d)(e) (vectors are plotted in every other x-grid point). This electric field is induced because the magnetic field tends to weaken as the reconnection proceeds. This negative electric field then produces the aforementioned negative current which

is mostly carried by the electrons due to large mobility along the magnetic field.

It is emphasized that the induced current J_y in the x-point region, which flows in the direction opposite to the flux tube current, blocks the incoming flux tube plasmas by repulsive force and impedes the magnetic reconnection. However, even if the sign of the E_y electric field (averaged over the diffusion layer) stays negative definite during the magnetic reconnection, the electron current J_{ey} in the same region does not change in response to this electric field. In fact, if we use $< E_y > \sim 3 \times 10^{-4} m_e c \omega_{pe}/e$ and $\tau \sim 1.6 \tau_A$ as a transit time, we should have $J_{ey} \cong n(e^2/m_e) < E_y > \tau \sim 9.8 \times 10^1$ which is about 150 times the observed value. This strongly implies occurrence of another process in the diffusion layer.

The current loss in the last paragraph is attributed to the non-MHD, poloidal electric field via the following mechanisms. One is an ejection of both the ions and electrons by the $E_x \hat{x} \times B_0 \hat{y}$ drift, and the other is a leakage of the accelerated electrons along the helical magnetic field. As already shown, the "diffusion layer" has become narrow enough at the commencement of magnetic reconnection so that the poloidal magnetic field becomes non-zero except for a thin layer through the x-point (Fig.3(e)). During the same period, the electric field E_x has been generated (Fig.3(d)). First, the super-Alfvenic flow by the $E \times B$ drift results from this electric field; the drift points laterally outward when viewed from the x-point. Consequently, the J_y current, hence, the magnetic flux rapidly convects into and out of the diffusion layer. Secondly, since $E_{\parallel} = (\mathbf{E} \cdot \mathbf{B})/B > 0$ as found by comparing Fig.3(d) and (e), the electrons are accelerated in the direction (anti-) parallel to the magnetic field to escape from the diffusion layer. This acceleration, which is found to supercede the one estimated by the E_y electric field, contributes to $\partial J_{\parallel}/\partial t > 0$ in the diffusion layer $(J_{\parallel}^{(0)} > 0)$.

The above statement is verified by tracing the particles in time. The marked particles that reside in a square region including the x-point at $t/\tau_A \cong 0.9$ deform to a dumbbell (dual-fan) shape in Fig.4, i.e., more number of particles populates with a distance from the x-point. Only a few marked particles are left in the vicinity of the x-point. This reveals that the particles are divided into two groups split at the x-point,

and that each group of particles proceeds laterally to either the positive or negative z-directions. On top of it, the electrons form two spiral arms that extend along the helical magnetic field. Since the arms develop in a clockwise direction with time, they consist of the electrons that have been accelerated to the negative y-direction by the parallel electric field $E_{\parallel}$ (> 0). Quantitatively, the plasma outward velocity is obtained using the particles shown in Fig.4. The average velocity just before the onset of the reconnection, $0.9 < t/\tau_A < 1.5$, is measured to be $<V_{ez}> \cong 1.2 <V_{ex}> \sim 0.012c$ for the electrons, and $<V_{iz}> \cong 0.78 <V_{ez}> \gg <V_{ix}>$. It is again found that the electrons move vertically as fast as they laterally do along the x-line. This is a remarkable difference from the ions which move preferentially by the $E \times B$ drift.

Thus far, the ion gyroradius was $\rho_i \cong 2c/\omega_{pe}$ ($\leq l_x$) for thermal ions. Other runs have been made with changing the ion temperature by an order of magnitude such that the ion gyroradius becomes $\rho_i \cong 0.6 \sim 6c/\omega_{pe}$. But, no appreciable change has been observed for the "magnetized" reconnection.

Theoretically, the collisionless dissipation of the x-point current required in magnetic reconnection may be understood in terms of the electron inertia. The electron momentum equation, $m_e(d\mathbf{v}_e/dt) = (-e)[\mathbf{E}+(\mathbf{v}_e/c)\times\mathbf{B}]-\nu m_e\mathbf{v}_e$, is ensemble-averaged to yield

$$\mathbf{E} = -\frac{\mathbf{V}_e}{c}\times\mathbf{B} + \eta\mathbf{J}_{e\parallel} + \frac{4\pi}{\omega_{pe}^2}\frac{d\mathbf{J}_{e\parallel}}{dt}, \tag{1}$$

where $\mathbf{J}_e = <(-e)n\mathbf{v}_e>$, $\mathbf{V}_e = <\mathbf{v}_e>$ and $\eta = 4\pi\nu/\omega_{pe}^2$. This is the equation used in the previous studies of weakly-collisional magnetic reconnection[1,2]. (But, Eq.(1) itself does not generate the quadrupole electrical potential.) Within this framework, the Faraday's law for the poloidal magnetic field may be approximated by

$$\frac{\partial\mathbf{B}_p}{\partial t} \cong -c\nabla\times\left\{\frac{4\pi}{\omega_{pe}^2}\left(\frac{\partial J_{e\parallel}}{\partial t} + (\mathbf{V}_e\cdot\nabla)J_{e\parallel}\right)\hat{y}\right\}, \tag{2}$$

in the diffusion layer of collisionless plasmas where $\eta \sim 0$. Since $E_{\parallel} > 0$ due to the quadrupole electric field, the terms in parentheses of Eq.(2) becomes positive definite. This results in $\partial\Psi/\partial t < 0$ which is the right sign for the flux tubes ($\Psi < 0$) to fill in

the diffusion layer between them. Thus, the parallel current due to the electron inertia is considered to play a decisive role in collisionless magnetic reconnection.

When the direction of the flux tube current is reversed with respect to the toroidal magnetic field, the excited poloidal electric field changes its sign. The plasma in the diffusion layer is ejected again outward, and the electron leakage occurs in the anti-clockwise direction along the helical magnetic field ($J_{\parallel}^{(0)} < 0,\ \partial J_{\parallel}/\partial t < 0$). For the reconnection in the magnetospheric neutral sheet, however, the toroidal magnetic field is absent[5,6]. The convection electric field is E_y in the present coordinate, and the charge redistribution that takes place in the magnetized reconnection is not expected. But, once the x-point region is charged negative, for example, by finite Larmor radius effect of ions, the electrons can be pulled out along the magnetic field, though its dissipation could be weaker[5].

In summary, we have shown in this paper that the collisionless dissipation for magnetic reconnection in magnetized plasmas is provided by linkage of the non-MHD, quadrupole electric field that is generated by the magnetic attraction of the bounded plasma, and resultant convection of plasma and magnetic flux by the $E \times B$ drift into and out of the diffusion layer and acceleration of the finite mass electrons along the helical magnetic field. For the above mechanism to be in effect, the presence of the toroidal magnetic field has been essential, as is the case with the magnetic island collapse in tokamaks and merging of the current filaments in the solar corona.

The author gratefully acknowledges valuable discussions with Dr.J.U.Brackbill, Dr.J.F.Drake, Dr.J.Todoroki, and Dr.H.Narita on discussions of magnetic reconnection and technique for ill-conditioned matrix inversion.

References

1. B.Coppi, Phys.Fluids, 8, 2273 (1965).
2. J.F.Drake, Phys.Fluids, 21, 1777 (1978); J.F.Drake and R.G.Kleva, Phys.Rev.Lett., 66, 1458 (1991).
3. A.Y.Aydemir, Phys.Fluids, B2, 2135 (1990).
4. T.Tajima, F.Brunel and J.Sakai, Astrophys.J., 258, L45 (1982).
5. R.Horiuchi and T.Sato, NIFS Report No. 233 (1993).
6. D.W.Hewett, G.E.Francis and L.E.Max, Phys.Rev.Lett., 61, 893 (1988).
7. M.Tanaka, J.Comput.Phys., 107, 124 (1993); ibid., 79, 209 (1988).
8. K.McGuire and TFTR team, Phys.Fluids, B2, 1287 (1990).
9. B.Coppi, S.Migliuolo, F.Pegoraro and F.Porcelli, Phys.Fluids, B2, 927 (1990).
10. J.H.Piddington, Cosmic Electrodynamics (Krieger Pub.Co., Florida, 1981).
11. H.X.Vu and J.U.Brackbill, Comput.Phys.Comm., 69, 253 (1992).
12. P.A.Sweet, Nuovo Cimento, 8, 188 (1958).
13. E.N.Parker, Astrophys.J.Suppl., 77, 177 (1963).

Figure Captions

FIG. 1. Development of poloidal magnetic flux function Ψ (top), and the y-component of ion current J_{iy} (bottom) for the times $t/\tau_A = (a)$ 0, (b) 1.6 and (c) 3.1.

FIG. 2. Time history of isolated poloidal flux $\Delta\Psi$ contained in a flux tube. The magnetic flux function is normalized as $e\Psi/m_e c^2$.

FIG. 3. (a) Electric field, (b) electrical potential, and (c) ion current at $t/\tau_A = 1.6$. Panel (d) and (e) are magnified plots of the central (x-point) region for the electric and magnetic fields, respectively. The electric and magnetic fields are normalized as $eE/m_e c\omega_{pe}$, and the maximum value is (d) 2.3×10^{-2}, and (e) 0.25.

FIG. 4. Particles occupying a square region at $t/\tau_A = 0.9$ (panel(a)) develop to the distribution for (b) ions and (c) electrons at $t/\tau_A = 1.9$.

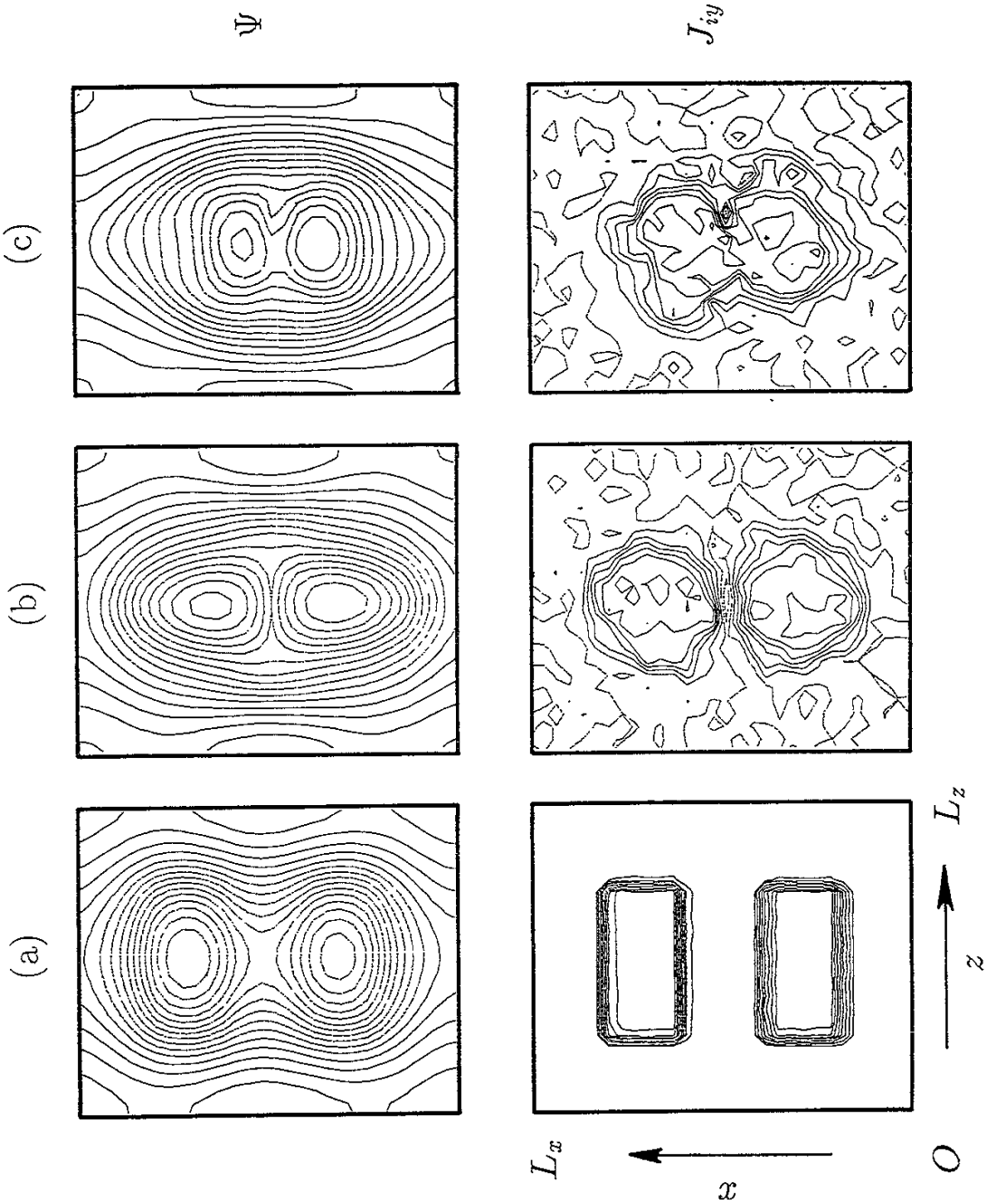

FIG. 1

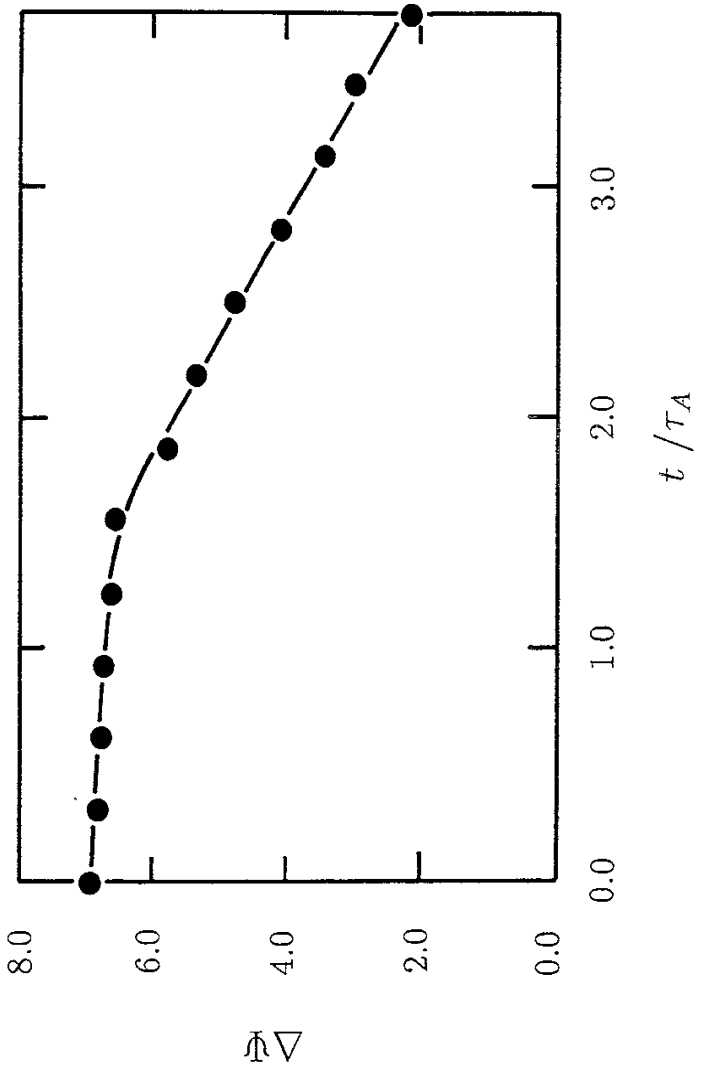

FIG. 2

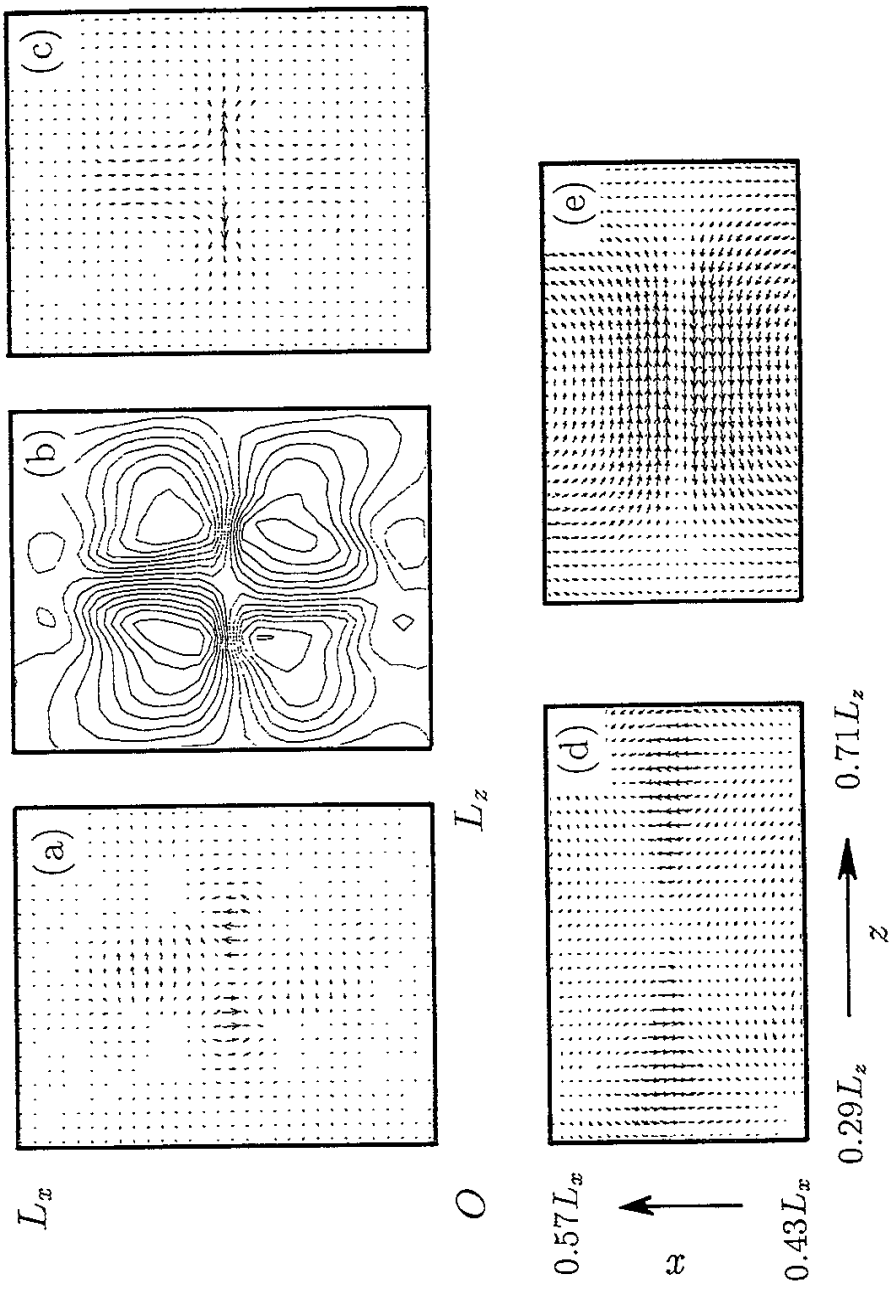

FIG. 3

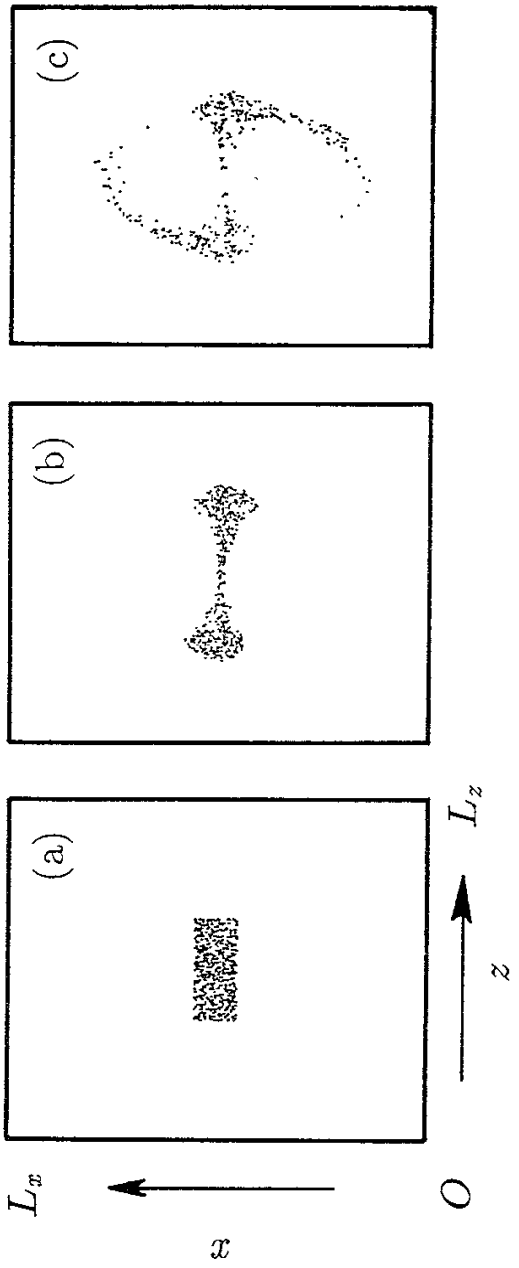

FIG. 4

Recent Issues of NIFS Series

NIFS-191 Y. Kondoh, Y. Hosaka and K. Ishii, *Kernel Optimum Nearly-Analytical Discretization (KOND) Algorithm Applied to Parabolic and Hyperbolic Equations* : Oct. 1992

NIFS-192 K. Itoh, M. Yagi, S.-I. Itoh, A. Fukuyama and M. Azumi, *L-Mode Confinement Model Based on Transport-MHD Theory in Tokamaks* ; Oct. 1992

NIFS-193 T. Watari, *Review of Japanese Results on Heating and Current Drive* ; Oct. 1992

NIFS-194 Y. Kondoh, *Eigenfunction for Dissipative Dynamics Operator and Attractor of Dissipative Structure* ; Oct. 1992

NIFS-195 T. Watanabe, H. Oya, K. Watanabe and T. Sato, *Comprehensive Simulation Study on Local and Global Development of Auroral Arcs and Field-Aligned Potentials* ; Oct. 1992

NIFS-196 T. Mori, K. Akaishi, Y. Kubota, O. Motojima, M. Mushiaki, Y. Funato and Y. Hanaoka, *Pumping Experiment of Water on B and LaB_6 Films with Electron Beam Evaporator* ; Oct., 1992

NIFS-197 T. Kato and K. Masai, *X-ray Spectra from Hinotori Satellite and Suprathermal Electrons* ; Oct. 1992

NIFS-198 K. Toi, S. Okamura, H. Iguchi, H. Yamada, S. Morita, S. Sakakibara, K. Ida, K. Nishimura, K. Matsuoka, R. Akiyama, H. Arimoto, M. Fujiwara, M. Hosokawa, H. Idei, O. Kaneko, S. Kubo, A. Sagara, C. Takahashi, Y. Takeiri, Y. Takita, K. Tsumori, I. Yamada and H. Zushi, *Formation of H-mode Like Transport Barrier in the CHS Heliotron / Torsatron* ; Oct. 1992

NIFS-199 M. Tanaka, *A Kinetic Simulation of Low-Frequency Electromagnetic Phenomena in Inhomogeneous Plasmas of Three-Dimensions* ; Nov. 1992

NIFS-200 K. Itoh, S.-I. Itoh, H. Sanuki and A. Fukuyama, *Roles of Electric Field on Toroidal Magnetic Confinement*, Nov. 1992

NIFS-201 G. Gnudi and T. Hatori, *Hamiltonian for the Toroidal Helical Magnetic Field Lines in the Vacuum*; Nov. 1992

NIFS-202 K. Itoh, S.-I. Itoh and A. Fukuyama, *Physics of Transport Phenomena in Magnetic Confinement Plasmas*; Dec. 1992

NIFS-203 Y. Hamada, Y. Kawasumi, H. Iguchi, A. Fujisawa, Y. Abe and M. Takahashi, *Mesh Effect in a Parallel Plate Analyzer*; Dec. 1992

NIFS-204 T. Okada and H. Tazawa, *Two-Stream Instability for a Light Ion Beam -Plasma System with External Magnetic Field;* Dec. 1992

NIFS-205 M. Osakabe, S. Itoh, Y. Gotoh, M. Sasao and J. Fujita, *A Compact Neutron Counter Telescope with Thick Radiator (Cotetra) for Fusion Experiment*; Jan. 1993

NIFS-206 T. Yabe and F. Xiao, *Tracking Sharp Interface of Two Fluids by the CIP (Cubic-Interpolated Propagation) Scheme*, Jan. 1993

NIFS-207 A. Kageyama, K. Watanabe and T. Sato, *Simulation Study of MHD Dynamo : Convection in a Rotating Spherical Shell*; Feb. 1993

NIFS-208 M. Okamoto and S. Murakami, *Plasma Heating in Toroidal Systems*; Feb. 1993

NIFS-209 K. Masai, *Density Dependence of Line Intensities and Application to Plasma Diagnostics*; Feb. 1993

NIFS-210 K. Ohkubo, M. Hosokawa, S. Kubo, M. Sato, Y. Takita and T. Kuroda, *R&D of Transmission Lines for ECH System* ; Feb. 1993

NIFS-211 A. A. Shishkin, K. Y. Watanabe, K. Yamazaki, O. Motojima, D. L. Grekov, M. S. Smirnova and A. V. Zolotukhin, *Some Features of Particle Orbit Behavior in LHD Configurations*; Mar. 1993

NIFS-212 Y. Kondoh, Y. Hosaka and J.-L. Liang, *Demonstration for Novel Self-organization Theory by Three-Dimensional Magnetohydrodynamic Simulation*; Mar. 1993

NIFS-213 K. Itoh, H. Sanuki and S.-I. Itoh, *Thermal and Electric Oscillation Driven by Orbit Loss in Helical Systems*; Mar. 1993

NIFS-214 T. Yamagishi, *Effect of Continuous Eigenvalue Spectrum on Plasma Transport in Toroidal Systems*; Mar. 1993

NIFS-215 K. Ida, K. Itoh, S.-I.Itoh, Y. Miura, JFT-2M Group and A. Fukuyama, *Thickness of the Layer of Strong Radial Electric Field in JFT-2M H-mode Plasmas*; Apr. 1993

NIFS-216 M. Yagi, K. Itoh, S.-I. Itoh, A. Fukuyama and M. Azumi, *Analysis of Current Diffusive Ballooning Mode*; Apr. 1993

NIFS-217 J. Guasp, K. Yamazaki and O. Motojima, *Particle Orbit Analysis for LHD Helical Axis Configurations* ; Apr. 1993

NIFS-218 T. Yabe, T. Ito and M. Okazaki, *Holography Machine HORN-1 for Computer-aided Retrieve of Virtual Three-dimensional Image* ; Apr. 1993

NIFS-219 K. Itoh, S.-I. Itoh, A. Fukuyama, M. Yagi and M. Azumi, *Self-sustained Turbulence and L-Mode Confinement in Toroidal Plasmas* ; Apr. 1993

NIFS-220 T. Watari, R. Kumazawa, T. Mutoh, T. Seki, K. Nishimura and F. Shimpo, *Applications of Non-resonant RF Forces to Improvement of Tokamak Reactor Performances Part I: Application of Ponderomotive Force* ; May 1993

NIFS-221 S.-I. Itoh, K. Itoh, and A. Fukuyama, *ELMy-H mode as Limit Cycle and Transient Responses of H-modes in Tokamaks* ; May 1993

NIFS-222 H. Hojo, M. Inutake, M. Ichimura, R. Katsumata and T. Watanabe, *Interchange Stability Criteria for Anisotropic Central-Cell Plasmas in the Tandem Mirror GAMMA 10 ;* May 1993

NIFS-223 K. Itoh, S.-I. Itoh, M. Yagi, A. Fukuyama and M. Azumi, *Theory of Pseudo-Classical Confinement and Transmutation to L-Mode;* May 1993

NIFS-224 M. Tanaka, *HIDENEK: An Implicit Particle Simulation of Kinetic-MHD Phenomena in Three-Dimensional Plasmas;* May 1993

NIFS-225 H. Hojo and T. Hatori, *Bounce Resonance Heating and Transport in a Magnetic Mirror;* May 1993

NIFS-226 S.-I. Iton, K. Itoh, A. Fukuyama, M. Yagi, *Theory of Anomalous Transport in H-Mode Plasmas;* May 1993

NIFS-227 T. Yamagishi, *Anomalous Cross Field Flux in CHS ;* May 1993

NIFS-228 Y. Ohkouchi, S. Sasaki, S. Takamura, T. Kato, *Effective Emission and Ionization Rate Coefficients of Atomic Carbons in Plasmas;* June 1993

NIFS-229 K. Itoh, M. Yagi, A. Fukuyama, S.-I. Itoh and M. Azumi, *Comment on 'A Mean Field Ohm's Law for Collisionless Plasmas;* June 1993

NIFS-230 H. Idei, K. Ida, H. Sanuki, H. Yamada, H. Iguchi, S. Kubo, R. Akiyama, H. Arimoto, M. Fujiwara, M. Hosokawa, K. Matsuoka, S. Morita, K. Nishimura, K. Ohkubo, S. Okamura, S. Sakakibara, C. Takahashi, Y. Takita, K. Tsumori and I. Yamada, *Transition of Radial Electric Field by Electron Cyclotron Heating in Stellarator Plasmas;* June 1993

NIFS-231 H.J. Gardner and K. Ichiguchi, *Free-Boundary Equilibrium Studies for the Large Helical Device*, June 1993

NIFS-232 K. Itoh, S.-I. Itoh, A. Fukuyama, H. Sanuki and M. Yagi, *Confinement Improvement in H-Mode-Like Plasmas in Helical Systems*, June 1993

NIFS-233 R. Horiuchi and T. Sato, *Collisionless Driven Magnetic Reconnection*, June 1993

NIFS-234 K. Itoh, S.-I. Itoh, A. Fukuyama, M. Yagi and M. *Azumi, Prandtl Number of Toroidal Plasmas;* June 1993

NIFS-235 S. Kawata, S. Kato and S. Kiyokawa , *Screening Constants for Plasma;* June 1993

NIFS-236 A. Fujisawa and Y. Hamada, *Theoretical Study of Cylindrical Energy Analyzers for MeV Range Heavy Ion Beam Probes;* July 1993

NIFS-237 N. Ohyabu, A. Sagara, T. Ono, T. Kawamura and O. Motojima, *Carbon Sheet Pumping;* July 1993

NIFS-238 K. Watanabe, T. Sato and Y. Nakayama, *Q-profile Flattening due to Nonlinear Development of Resistive Kink Mode and Ensuing Fast Crash in Sawtooth Oscillations;* July 1993

NIFS-239 N. Ohyabu, T. Watanabe, Hantao Ji, H. Akao, T. Ono, T. Kawamura, K. Yamazaki, K. Akaishi, N. Inoue, A. Komori, Y. Kubota, N. Noda, A. Sagara, H. Suzuki, O. Motojima, M. Fujiwara, A. Iiyoshi, *LHD Helical Divertor;* July 1993

NIFS-240 Y. Miura, F. Okano, N. Suzuki, M. Mori, K. Hoshino, H. Maeda, T. Takizuka, JFT-2M Group, K. Itoh and S.-I. Itoh, *Ion Heat Pulse after Sawtooth Crash in the JFT-2M Tokama;* Aug. 1993

NIFS-241 K. Ida, Y.Miura, T. Matsuda, K. Itoh and JFT-2M Group, *Observation of non Diffusive Term of Toroidal Momentum Transport in the JFT-2M Tokamak;* Aug. 1993

NIFS-242 O.J.W.F. Kardaun, S.-I. Itoh, K. Itoh and J.W.P.F. Kardaun, *Discriminant Analysis to Predict the Occurrence of ELMS in H-Mode Discharges;* Aug. 1993

NIFS-243 K. Itoh, S.-I. Itoh, A. Fukuyama, *Modelling of Transport Phenomena;* Sep. 1993

NIFS-244 J. Todoroki, *Averaged Resistive MHD Equations;* Sep. 1993